Discrimination of melanoma cell lines with Fourier Transform Infrared (FTIR) spectroscopy

Bijay Ratna Shakya[a], Hanna-Riikka Teppo[b,c,d], Lassi Rieppo[a*]

[a] *Research Unit of Medical Imaging, Physics and Technology, Faculty of Medicine, University of Oulu, Oulu, Finland*

[b] *Cancer Research and Translational Medicine Research Unit, University of Oulu, Oulu, Finland*

[c] *Department of Pathology, Oulu University Hospital, Oulu, Finland*

[d] *Medical Research Center Oulu, Oulu University Hospital and University of Oulu, Finland*

Abstract

Among skin cancers, melanoma is the lethal form and the leading cause of death in humans. Melanoma begins in melanocytes and is curable at early stages. Thus, early detection and evaluation of its metastatic potential is crucial for effective clinical intervention. Fourier transform infrared (FTIR) spectroscopy has gained considerable attention due to its versatility in detecting biochemical and biological features present in the samples. Changes in these features are used to differentiate between samples at different stages of the disease. Previously, FTIR spectroscopy has been mostly used to distinguish between healthy and diseased conditions. With this study, we aim to discriminate between different melanoma cell lines based on their FTIR spectra. Formalin-fixed paraffin embedded samples from three melanoma cell lines (IPC-298, SK-MEL-30 and COLO-800) were used. Statistically significant differences were observed in the prominent spectral bands of three cell lines along with shifts in peak positions. Partial least square discriminant analysis (PLS-DA) models built for the classification of three cell lines showed accuracies of 96.38 %, 95.96 % and 99.7 %, for the differentiation of IPC-298, SK-MEL-30 and COLO-800, respectively. The results suggest that FTIR spectroscopy can be used to differentiate between genetically different melanoma cells and thus potentially characterize the metastatic potential of melanoma.

Introduction

Melanoma is the most fatal type of skin cancer and, therefore, it is responsible for the majority of skin cancer related deaths. Oncogenic transformation of melanocytes initiates the biological processes of melanoma followed by promotion and progression in the form of accumulative cellular damage, evasion of apoptosis and epithelial-to-mesenchymal transition (EMT). This EMT process involves detachment from cell contact, alteration of cell shape, expression of matrix degrading enzymes, increased motility and finally detachment from the primary tumour site and migration through the blood and lymphatic nodes indicating the high metastatic potential that may lead to the development secondary tumours [1, 2].

The diagnosis of melanoma is based on histomorphology and cytopathology of the tissue in haematoxylin-and-eosin (H&E) stained sections with adjunct histochemical and immunohistochemical staining. The stage or aggressiveness is then graded considering tumour thickness (Breslow index and Clark level), ulceration, mitotic rate, lymph node involvement and the distant metastasis status [3]. The concordance of histological diagnosis is only moderate in melanocytic lesions [4-6] and depends largely on the experience of pathologist. In addition to the morphological assessment of melanocytic tumours, Next-generation sequencing based analyses of the underlying genomic alterations are being developed and can be effective in the difficult intermediate category of melanocytic neoplasia [7].

Fourier Transform Infrared (FTIR) spectroscopy is based on absorption of infrared light by a sample at mid-infrared region. It probes structure, function and biochemical composition of cells and tissues. Compared with conventional histopathology, FTIR microscopy does not need any staining procedure prior to the measurement and can be performed directly on paraffin-embedded cells or tissues. The analysis of acquired spectra can be automated using machine learning algorithms, making the classification of lesions less prone to operator errors. We have recently reviewed the efficacy of FTIR spectroscopy in skin cancer research [8]. FTIR spectroscopy has been previously shown to discriminate between healthy and diseased conditions of various skin cancers [9-12]. It has also been used to evaluate the effectiveness of drugs for treating melanoma [13]. Furthermore, Fourier Transform Infrared attenuated total reflectance (FTIR-ATR) modality has been used to assess the metastatic potential of live melanoma cells based on their membrane hydration level [14]. However, this procedure is

not applicable to commonly used formalin-fixed paraffin-embedded (FFPE) biopsy samples. To our knowledge, no model has yet been developed to characterize the metastatic potential of fixed melanoma cells.

In this study, we aim to develop a model that can discriminate genetically different melanoma cells based on their FTIR spectra. The cells of the study are processed using the standard FFPE processing to make the results comparable with FFPE biopsy samples.

Materials and methods

Cell lines

Three melanoma cell lines, IPC-298 (ACC 251), SK-MEL-30 (ACC 151) and COLO-800 (ACC 193), were purchased from Leibniz-Institut DSMZ (Braunschweig, Germany) and used in this study. The melanoma cell line IPC-298 is derived from a primary melanoma tumour of a 64-year-old female, SK-MEL-30 is derived from a subcutaneous metastasis of a 67-year-old male with melanoma, and COLO-800 is derived from a subcutaneous nodule of a 14 year old male with melanoma. The cell lines were cultured in RPMI-1640 with 10% fetal bovine serum and 100 IU/ml penicillin and streptomycin (Pen-Strep solution HyClone laboratories, Inc. Utah, USA SV30010.01). The cells were fixed with formalin for 30 minutes on the cell culture plate, and then the cells were scraped and centrifuged. The resulting cell pellet was mixed with 1.5% agar followed by the paraffin embedding procedure. Subsequently, 5-µm-thick sections were cut and placed on 2-mm-thick CaF_2 windows for FTIR spectroscopic analysis. Paraffin was dissolved with xylene before the FTIR microscopy measurements.

FTIR data acquisition

Nicolet iN10 MX (Thermo Scientific, Wisconsin, MA, USA) FTIR microscope was used for the acquisition of spectra. A nitrogen-cooled mercury cadmium telluride (MCT) detector was used for the measurements. Two sections from each cell line were used in the study. The total of 260 cells spectra were acquired from IPC-298 cell line (primary melanoma) while 300 and 260 cells spectra were acquired from SK-MEL-30 and COLO-800 cell lines (metastatic melanoma), respectively. Before each acquisition, a background spectrum was collected from a clean CaF_2 window and was automatically subtracted from each cell spectrum. The spectra were collected in transmission mode, and one absorbance spectrum for each cell (aperture size: 20

×20 μm^2) was collected using the spectral range of 900-4000 cm^{-1} with a spectral resolution of 8 cm^{-1}. It took about 4 minutes to acquire spectrum of each cell with 256 scans (including the collection of background spectrum, which was also acquired with 256 scans).

Data pre-processing

For every spectrum, a simple offset correction for baseline was conducted prior to resonant Mie scattering correction (RMieS) to remove any negative values. Thereafter, RMieS algorithm [15] was applied to the spectra to remove alterations due to scattering of infrared radiation from the cells. The number of iterations was set to five while the other correction options for the RMieS algorithm were set to the default values. After RMieS correction, spectra were normalized using vector normalization. The mean spectra of three cell lines after normalization are shown in Figure 1. The first derivatives were then calculated using Savitzky-Golay algorithm (smoothing points = 9). Since the spectral features of paraffin remnants can often still be seen in the acquired spectra of deparaffinised samples [16], the lipid (2835-2999cm^{-1}) and CH_3 (1351-1480 cm^{-1}) region were truncated from further analysis as these regions are mostly affected by paraffin [17]. In addition, the non-absorbing regions (1801-2834 cm^{-1} and 3631-4000 cm^{-1}) were also removed from the spectra and then used in multivariate analysis (Figure 2). All processing was done in MATLAB (R2017b, MathWorks, Natick, MA, USA).

Data analysis

Firstly, the mean spectrum of each cell line was generated by averaging all spectra acquired from each cell line after required pre-processing procedures (baseline correction, RMieS correction and normalization) to visualize the spectral differences between the cell lines. The mean spectra consisted of multiple peaks associated with vibrational modes of molecules within the samples. The intensity and position of these peaks depend on the biochemical molecule (e.g. proteins, lipids and nucleic acid), their structure and conformation, and their intermolecular relationships [18]. To interpret the differences in the prominent spectral bands between the three cell lines, the integrated areas of the peaks of interest were calculated and their possible peak shifts were evaluated. Along with these peaks, amide I/amide II ratio was calculated by dividing the integrated area of amide I by the integrated area of amide II. Furthermore, one-way ANOVA test was performed and the pairwise

comparison between each cell line was conducted using Bonferroni method to evaluate the significance of the differences of these bands between the cell lines. The limit of statistical significance was set at $p < 0.05$.

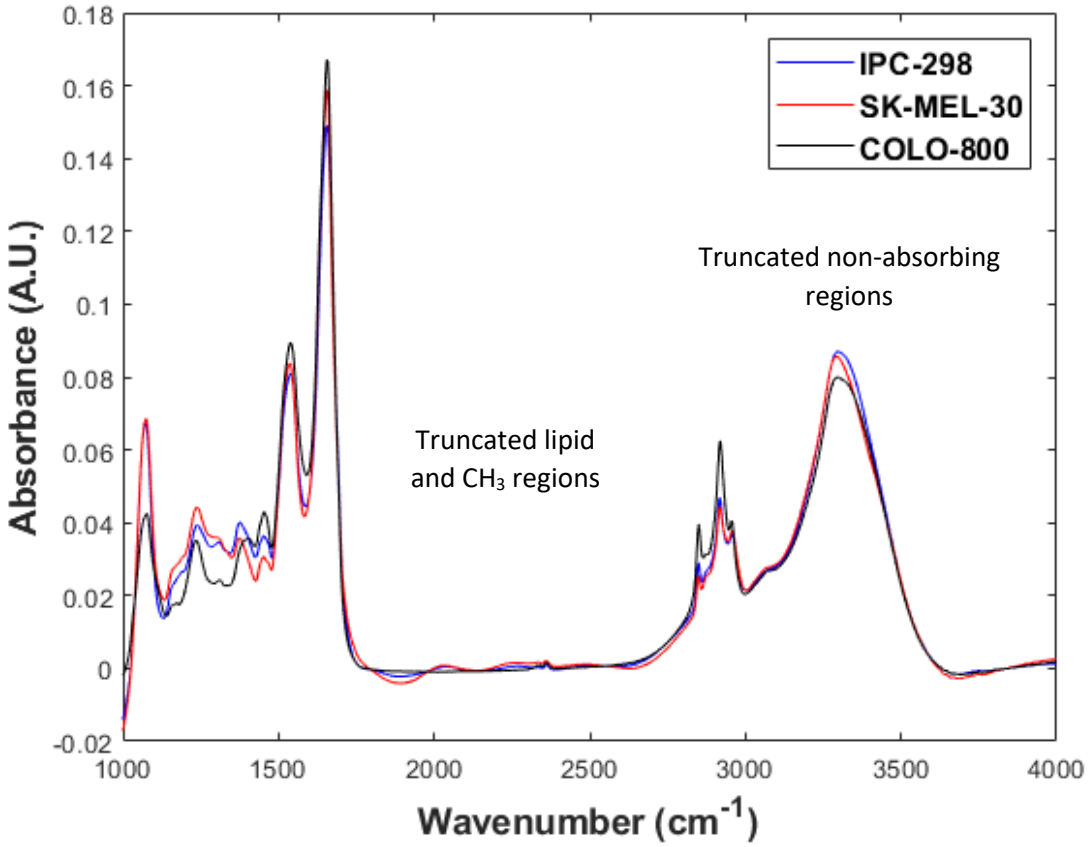

Figure 1: Mean spectra of metastatic melanoma cells (SK-MEL-30: red and COLO-800: black) and primary melanoma cells (IPC-298: blue).

In order to observe differences between cell lines, Principal Component Analysis (PCA) was performed on the first derivative spectra of the three cell lines. PCA does not use any *a priori* information about the classes of spectra but considers only the variance in the spectral data. PCA reduces a large set of variables to a small set of new variables while preserving most of the information. The new variables, i.e. principal components (PCs), are ranked by the amount of variance they explain: the first PC accounts for the largest variance in data while each succeeding PC accounts for the remaining variability. The result of PCA is commonly evaluated based on the scores of first two or three PCs. In addition, the Partial Least Squares Discriminant Analysis (PLS-DA) models were built for supervised classification between the first derivative spectra of the three melanoma cell lines. In total, three models were built to detect each cell line. The first model was used to differentiate IPC-298 from SK-MEL-30 and

COLO-800. In this model, the spectra of IPC-298 were used as one class and the spectra of SK-MEL-30 + COLO-800 were grouped into another class. Similarly, SK-MEL-30 and COLO-800 were used as one class in the second and third models while IPC-298 + COLO-800 and IPC-298 + SK-MEL-30 were grouped into another class. In the training phase, PLS-DA utilizes *a priori* knowledge about the classes of spectra of the training data set to determine the differences between the studied groups. A separate test set is then used to validate the trained model. PLS-DA models were built using 60% of the spectra from each cell line for training the model, while the remaining 40% were used as the test set. The models were run 25 times, and each time the spectra were randomly assigned to training set and test set.

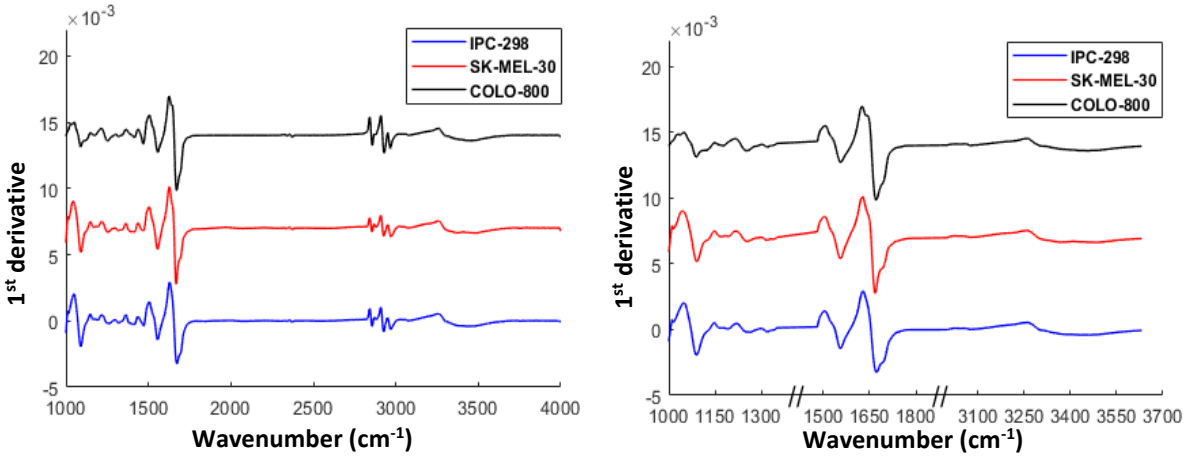

Figure 2: (a) Mean first derivative spectra of primary melanoma cells (IPC-298: blue) and metastatic melanoma cells (SK-MEL-30: red and COLO-800: black). (b) Truncated first derivate spectra used for classification model. Offset values of 0.007 and 0.014 were added to SK-MEL-30 and COLO-800 cell line spectra, respectively, while plotting the figure to avoid overlap between the spectra.

Results

The FTIR spectra of the melanoma cell lines were investigated in the region 1000-4000 cm^{-1}. The mean spectra (after required pre-processing) of the three malignant melanoma cell lines are presented in Figure 1. The spectra can be divided in three zones. In the first zone, i.e. the range of 1000-1480 cm^{-1}, the absorption is mainly due to the cellular constituents of carbohydrates, nucleic acids and phosphates. The four prominent spectral bands in this region were observed at 1072, 1238, 1373 and 1450 cm^{-1}. The bands at 1072 and 1238 cm^{-1} are symmetric and antisymmetric phosphate stretching vibration bands of nucleic acids and phospholipids. The band at 1373 cm^{-1} occurs due to symmetric vibrations of carboxylate functionals groups in protein (ν_s C=O), while band at 1450 cm^{-1} is due to symmetric bending

of CH_2 in lipids ($\delta_s CH_2$). In the range of 1481-1800 cm^{-1}, the main protein bands, i.e., amide II at 1539 and amide I at 1655 cm^{-1}, are observed. Amide I arise from C=O stretching vibration of peptide backbone and coupling of C-N vibration, while amide II is mainly due to C=O stretching vibration and coupling of N-H bending modes. The last zone, i.e. the range of 2835-3630 cm^{-1}, results from the absorption of lipids and N-H amino group. The bands at 2850 cm^{-1} and 2877 cm^{-1} arise from symmetric stretching of the methylene ($\nu_s CH_2$) and methyl ($\nu_s CH_3$) chains, respectively, in membrane lipids, while the bands at 2916 cm^{-1} and 2958 cm^{-1} are due to antisymmetric stretching of methylene ($\nu_{as} CH_2$) and methyl groups ($\nu_{as} CH_3$) respectively of both lipids and proteins. The last prominent band observed at 3298 cm^{-1} is amide A which occurs due to stretching vibration of NH groups of proteins. The prominent spectral bands are well characterized by all cell lines. [8]

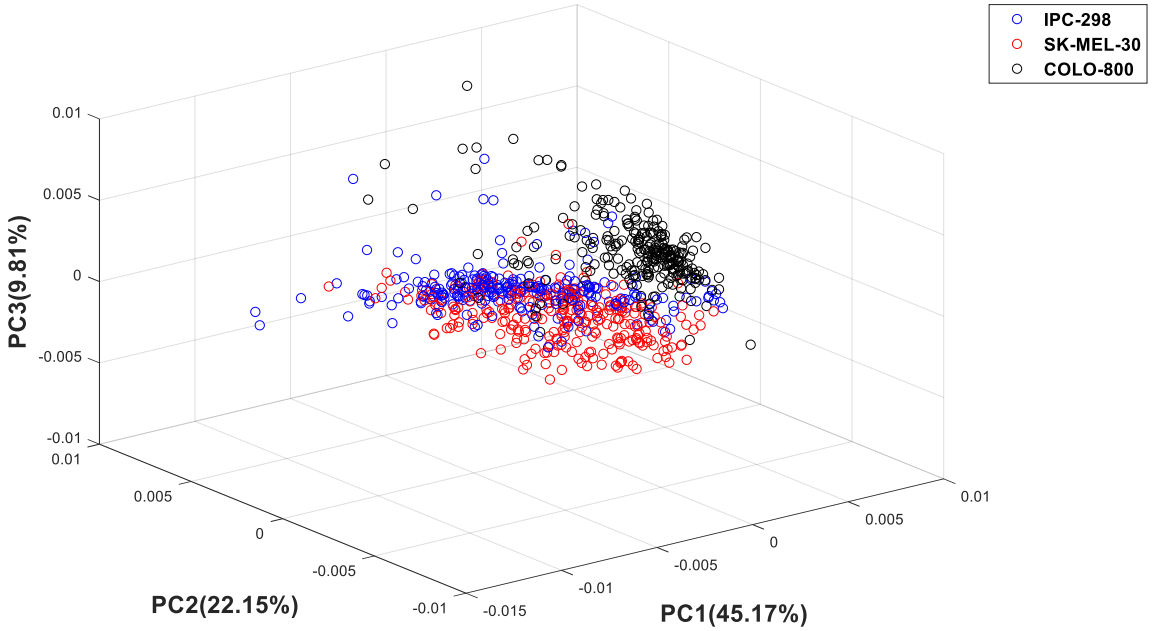

Figure 3: Three-dimensional score plot computed using first three PCs. The primary melanoma cells (IPC-298) are marked with blue circles and the metastatic melanoma cells: SK-MEL-30 and COLO-800 with red and black circles respectively.

The spectra of the three melanoma cell lines show differences in integrated absorbances of prominent bands as well as band positions. Compared with COLO-800 cell line, IPC-298 and SK-MEL-30 cell lines showed higher absorbance in phosphate (symmetric and antisymmetric) bands. Increase in the absorbance intensities of amide I and amide II bands were observed in metastatic cell lines compared with primary, suggesting alteration in native protein

structure. The opposite was observed in amide A region where absorbance was weaker in the metastatic cell line. Compared with IPC-298, band shift to lower wavenumbers were observed in antisymmetric phosphate band of COLO-800 cell line (from 1238 to 1234 cm^{-1}), while in SK-MEL-30, amide II peak shifted from 1539 to 1535 cm^{-1}. Amide A band of both metastatic cell lines also shifted to a lower wavenumber (from 3298 to 3294 cm^{-1}).

Table 1: Wavenumbers of observed spectral bands with their integrated area for statistical comparison.

Peak assignment	**Band Positions**			**Integrated area (mean)**		
	Primary (IPC-298)	Metastatic (SK-MEL-30)	Metastatic (COLO-800)	Primary (IPC-298)	Metastatic (SK-MEL-30)	Metastatic (COLO-800)
Phosphate (symmetric)	1072	1072	1072	3.5159	3.6307	2.0915
Phosphate (antisymmetric)	1238	1238	1234	0.3414	0.3985	0.4919
Amide II	1539	1535	1539	2.2874	2.6308	2.4117
Amide I	1655	1655	1655	6.8677	7.4074	6.8480
Amide A	3298	3294	3294	17.0826	16.6342	15.7563

The phosphate and amide contents were calculated by measuring the integrated area of symmetric phosphate stretching (1000-1130 cm^{-1}), antisymmetric phosphate stretching (1200-1273 cm^{-1}), amide I (1585-1765 cm^{-1}), amide II (1481-1581 cm^{-1}) and amide A (3070-3630 cm^{-1}) bands for all melanoma cell lines. Statistically significant differences were observed between each cell line in phosphate (antisymmetric), amide II and amide A bands. In phosphate (symmetric) and amide I bands, no significant differences were observed while comparing IPC-298 vs SK-MEL-30 or IPC-298 vs COLO-800 cell lines, but the remaining comparisons showed significant differences in these bands as well. Moreover, amide I/amide II ratio showed a significant difference between the primary and metastatic cell lines, but no significant difference was observed between the two metastatic cell lines. The peak positions

of prominent spectral bands along with their integrated area are shown in Table 1 while the pairwise comparisons of each cell line are shown in Table 2.

Table 2: One-way ANOVA test for the prominent spectral bands between three malignant melanoma cell lines.

Peak Assignment	**Comparison between cell lines**	**Mean difference**	***p*-value***
Phosphate (symmetric)	IPC-298 and SK-MEL-30	0.11 ± 0.082	0.93
	IPC-298 and COLO-800	1.42 ± 0.077	<0.0001
	SK-MEL-30 and COLO-800	1.53 ± 0.082	<0.0001
Phosphate (antisymmetric)	IPC-298 and SK-MEL-30	0.05 ± 0.007	<0.0001
	IPC-298 and COLO-800	0.15 ± 0.007	<0.0001
	SK-MEL-30 and COLO-800	0.09 ± 0.007	<0.0001
Amide II	IPC-298 and SK-MEL-30	0.34 ± 0.023	<0.0001
	IPC-298 and COLO-800	0.12 ± 0.021	0.0005
	SK-MEL-30 and COLO-800	0.21 ± 0.023	<0.0001
Amide I	IPC-298 and SK-MEL-30	0.53 ± 0.029	<0.0001
	IPC-298 and COLO-800	0.01 ± 0.027	1
	SK-MEL-30 and COLO-800	0.55 ± 0.029	<0.0001
Amide A	IPC-298 and SK-MEL-30	0.44 ± 0.087	0.0006
	IPC-298 and COLO-800	1.32 ± 0.081	<0.0001
	SK-MEL-30 and COLO-800	0.87 ± 0.087	<0.0001
Amide I/ Amide II	IPC-298 and SK-MEL-30	0.19 ± 0.021	<0.0001
	IPC-298 and COLO-800	0.17 ± 0.020	<0.0001
	SK-MEL-30 and COLO-800	0.02 ± 0.021	1

*Differences between each cell lines using Bonferroni test.

PCA was applied to all acquired spectra in the region 1000-4000 cm^{-1} (excluding paraffin affected and non-absorbing regions, i.e., 1351-1480 cm^{-1}, 1801-2999 cm^{-1} and 3631-4000 cm^{-1}). The first three PCs accounting for almost 80% of variance (PC1: 45.17%, PC2: 22.15%, PC3: 9.81%) were used to explore the spectral differences in an unsupervised manner. In Figure 3, each point in the plot represents the transformed variable values of each spectrum known as scores. As seen in Figure 3, three clusters are formed with some degree of separation, but there is still significant overlap between the three cell lines.

To better classify the spectra of each cell line, PLS-DA models were created. The models showed high recognition rate with the mean sensitivities of 93.35%, 97.40%, 99.14% and the mean specificities of 97.81%, 95.16%, 99.95% for IPC-298, SK-MEL-30 and COLO-800, respectively. The predicted results for the test data set for each cell line are shown in tables 3. The predicted results are represented as the mean (± SD) percentages of the classification accuracy.

Discussion

In this study, we evaluated the potential of FTIR spectroscopy for differentiating three melanoma cell lines processed using FFPE protocol. Firstly, the univariate analysis was used to show significant differences in integrated absorbances of phosphate (antisymmetric), phosphate (symmetric), amide I, amide II and amide A bands, between the FTIR spectra of each cell line. Then, multivariate analysis, i.e. PCA and PLS-DA, was performed for further discrimination. The developed PLS-DA models can accurately (>95%) differentiate each cell line from the remaining two cell lines grouped together. The result also suggests the possibility of differentiating primary melanoma cells from the metastatic melanoma cells with FTIR spectroscopy, but this requires further testing with larger sample sets.

Often the cell studies are done by using only e.g. air drying for fixation. We opted to use FFPE processing as it is commonly applied to biopsy samples to preserve the sample and give support during sectioning. In FFPE samples, paraffin is usually chemically eliminated prior to FTIR spectroscopic measurements because of its intense vibration bands near the lipid (2835-3000cm^{-1}) and CH_3 (1350-1477 cm^{-1}) regions. However, as it can be difficult to remove paraffin completely with organic solvents, we decided to remove the potentially paraffin-affected regions completely from the spectra. The accurate classification of FFPE processed primary

and metastatic melanoma cells is a promising sign for the future studies where the metastatic potential of melanoma cells would be assessed from FFPE processed skin biopsies.

Table 3: Recognition of each cell line from remaining two cell lines grouped together with the PLS-DA model. The results are the average of 25 PLS-DA runs with random training/test set splits.

For IPC-298		
Predicted as / Cell type	IPC-298	SK-MEL-30 + COLO-800
IPC-298	93.35 ± 2.44	6.64 ± 2.44
SK-MEL-30 + COLO-800	2.18 ± 1.21	97.81 ± 1.21
For SK-MEL-30		
Predicted as / Cell type	SK-MEL-30	IPC-298 + COLO-800
SK-MEL-30	97.40 ± 1.49	2.59 ± 1.49
IPC-298 + COLO-800	4.84 ± 1.35	95.16 ± 1.35
For COLO-800		
Predicted as / Cell type	COLO-800	IPC-298 + SK-MEL-30
COLO-800	99.14 ± 0.69	0.86 ± 0.69
IPC-298 + SK-MEL-30	0.04 ± 0.13	99.95 ± 0.13

In our study, we observed high amide I and amide II absorbances for metastatic cells compared with primary melanoma cells. The increase in these absorbances may be due to change in membrane hydration level, which is caused due to increased fluidity in cells. Cells with high metastatic potential are observed to have high membrane fluidity which in turn is responsible for higher hydration level in the cells [19, 20]. According to an earlier study, the increase in hydration level is associated with the increase in amide I and amide II absorbances [21]. In addition, Minnes *et al.* [14] showed increased absorption intensity of protein and change in intermolecular structure of water molecules with increasing metastatic potential.

We observed a statistically significant difference in the integrated absorbance of amide I and amide II peaks between the cell lines. Additionally, there was a shift of amide II band to a lower wavenumber in metastatic cells. This is mainly due to changes in secondary protein structure which is potentially related to the increased metastatic potential.

Another significant spectral variation was observed in phosphate bands. Asymmetrical phosphate band showed increased absorbance in metastatic cells. These phosphate stretching bands arise from the phosphodiester group of nucleic acids and can provide information on various states of cells [22]. These changes indicate the alteration of environment near phosphate group, which may have been caused due to change in hydration level of cells and affecting the hydration in vicinity of nucleic acid. This causes changes in DNA and proliferative capacity of cells which are expected in metastatic condition.

Amide A region also showed significant spectral variation between the cell types. This band corresponds to N-H stretching vibration in proteins. The decrease in absorbance of this band is observed with increasing metastatic potential of cells. Moreover, the considerable shift in the position of this band to a lower wavenumber was observed in metastatic cells. These changes are caused due to the increasing of hydrogen bonding of the affected secondary amino function in metastatic cells [23]. These hydrogen bonds are important in stabilizing the protein helix structure. The change in these structures indicate the alteration of physiological environment.

PCA was carried out on all acquired malignant melanoma cell spectra. Successful separation of cell lines using this multivariate methodology would have been encouraging as it is an unsupervised method and does not need any prior knowledge for classification. However, the result from the analysis showed a limited separation with a significant overlap between the three cell lines. A good classification was achieved for discriminating between different melanoma cell lines using PLS-DA. The three developed models were able to predict each cell line with high sensitivity and specificity with mean accuracies of 96.38%, 95.96% and 99.7%, respectively. In addition, the developed model also discriminated between primary and metastatic melanoma cells, suggesting the possibility of using FTIR spectroscopy with a developed model to characterize the metastatic behaviour. Despite this promising result, challenges with the separation remain. Cells in the primary tumour site and metastatic lesion are likely to be very similar phenotypically [24] and genetically [25] as mutational spectra is

highly similar in matched primary and metastatic acral melanomas [26]. It remains unclear which cell dependent and microenvironmental factors contribute the most to the classification. In a study by Wald et al. [24], melanoma cells in the primary tumour and in metastasis were compared using FFPE tissue microarray sections. Neither supervised nor unsupervised analysis were able to reveal significant differences between the two classes. However, they were able to differentiate between batched primary tumours of patients at stage I or II (non-metastatic stages) and batched primary tumours of patients at stage III or IV (metastatic stages).

When a tumour develops, it undergoes a number of genomic alterations and becomes heterogeneous during the progression of the disease due to genetic, transcriptomic, pregenetic and phenotypic changes [27]. Genomic alterations differ among patients but also within the primary tumour and between the primary and metastatic lesion leading to intratumoral and intertumoral heterogeneity. Furthermore, metastatic cells can acquire new mutations and develop independently, known as intermetastatic heterogeneity [28]. These heterogeneities might explain the high level of irreproducibility of cancer research. The progression of melanoma into a metastatic pool of cells is greatly influenced by the tumour microenvironment, which is able to modulate various phenotypes reflecting to therapy resistance [29]. Single cell analysis has recently been recognized as the best approach to study intratumoral heterogeneity, but in contrast to FTIR spectroscopy, it would be difficult to implement it on routine basis for diagnostics [30].

Although our study shows promising results in discriminating malignant melanoma cell lines, it has some limitations. Firstly, only three cell lines were included in the study and secondly, our samples consist of only cultured melanoma cells. Furthermore, the cell lines used in the study are from different patients without the same biological features and clinical evolution. In the future, the similar approach should be taken with biopsy samples, which are commonly used for histopathological inspection, encompassing of various other skin cells. This will reveal the real efficiency of the FTIR spectroscopic assessment of the metastatic potential of melanoma cells and tumour heterogeneity.

In conclusion, we observed significant differences between the FTIR spectra of different melanoma cell lines, and we were also able to discriminate between the cell lines with the

developed PLS-DA models. The results encourage continuing the research towards development of FTIR spectroscopic assessment of melanomas from skin biopsies.

References

1. Eggermont, A.M., Spatz, A. and Robert, C. (2014) Cutaneous melanoma. *The Lancet.* **383,** 816-827.

2. Hodorogea, A., Calinescu, A., Antohe, M., Balaban, M., Nedelcu, R.I., Turcu, G., Ion, D.A., Badarau, I.A., Popescu, C.M. and Popescu, R. (2019) Epithelial-mesenchymal transition in skin cancers: a review. *Analytical Cellular Pathology.* **2019,**

3. Elder, D.E., Massi, D., Scolyer, R.A. and Willemze, R. (2018) WHO classification of skin tumours. International Agency for Research on Cancer, Lyon

4. Farmer, E.R., Gonin, R. and Hanna, M.P. (1996) Discordance in the histopathologic diagnosis of melanoma and melanocytic nevi between expert pathologists. *Hum. Pathol.* **27,** 528-531.

5. Elmore, J.G., Barnhill, R.L., Elder, D.E., Longton, G.M., Pepe, M.S., Reisch, L.M., Carney, P.A., Titus, L.J., Nelson, H.D., Onega, T., Tosteson, A.N.A., Weinstock, M.A., Knezevich, S.R. and Piepkorn, M.W. (2017) Pathologists' diagnosis of invasive melanoma and melanocytic proliferations: observer accuracy and reproducibility study. *BMJ.* **357,** j2813.

6. Elmore, J.G., Elder, D.E., Barnhill, R.L., Knezevich, S.R., Longton, G.M., Titus, L.J., Weinstock, M.A., Pepe, M.S., Nelson, H.D. and Reisch, L.M. (2018) Concordance and Reproducibility of Melanoma Staging According to the 7th vs 8th Edition of the AJCC Cancer Staging Manual. *JAMA network open.* **1,** e180083-e180083.

7. Shain, A.H., Yeh, I., Kovalyshyn, I., Sriharan, A., Talevich, E., Gagnon, A., Dummer, R., North, J., Pincus, L. and Ruben, B. (2015) The genetic evolution of melanoma from precursor lesions. *N. Engl. J. Med.* **373,** 1926-1936.

8. Shakya, B.R., Shrestha, P., Teppo, H. and Rieppo, L. (2020) The use of Fourier Transform Infrared (FTIR) spectroscopy in skin cancer research: a systematic review. *Applied Spectroscopy Reviews.* 1-33.

9. Kyriakidou, M., Anastassopoulou, J., Tsakiris, A., Koui, M. and Theophanides, T. (2017) FT-IR Spectroscopy Study in Early Diagnosis of Skin Cancer. *In Vivo.* **31,** 1131-1137.

10. Khanmohammadi, M., Nasiri, R., Ghasemi, K., Samani, S. and Garmarudi, A.B. (2007) Diagnosis of basal cell carcinoma by infrared spectroscopy of whole blood samples applying soft independent modeling class analogy. *J. Cancer Res. Clin. Oncol.* **133,** 1001-1010.

11. Hammody, Z., Argov, S., Sahu, R.K., Cagnano, E., Moreh, R. and Mordechai, S. (2008) Distinction of malignant melanoma and epidermis using IR micro-spectroscopy and statistical methods. *Analyst.* **133,** 372-378.

12. Bortoletto, D.R., Lima, C.A., Zezell, D., Sato, E.T. and Martinho, H. (2018) Vibrational spectra calculation of squamous cell carcinoma in the amide band region. *Vibrational Spectroscopy.* **97,** 135-139.

13. Wald, N., Le Corre, Y., Martin, L., Mathieu, V. and Goormaghtigh, E. (2016) Infrared spectra of primary melanomas can predict response to chemotherapy: The example of dacarbazine. *Biochimica Et Biophysica Acta-Molecular Basis of Disease.* **1862,** 174-181.

14. Minnes, R., Nissinmann, M., Maizels, Y., Gerlitz, G., Katzir, A. and Raichlin, Y. (2017) Using Attenuated Total Reflection-Fourier Transform Infra-Red (ATR-FTIR) spectroscopy to distinguish between melanoma cells with a different metastatic potential. *Scientific Reports.* **7,** 4381.

15. Bassan, P., Kohler, A., Martens, H., Lee, J., Byrne, H.J., Dumas, P., Gazi, E., Brown, M., Clarke, N. and Gardner, P. (2010) Resonant Mie scattering (RMieS) correction of infrared spectra from highly scattering biological samples. *Analyst.* **135,** 268-277.

16. Meuse, C.W. and Barker, P.E. (2009) Quantitative infrared spectroscopy of formalin-fixed, paraffin-embedded tissue specimens: paraffin wax removal with organic solvents. *Applied Immunohistochemistry & Molecular Morphology.* **17,** 547-552.

17. Tfayli, A., Piot, O., Durlach, A., Bernard, P. and Manfait, M. (2005) Discriminating nevus and melanoma on paraffin-embedded skin biopsies using FTIR micro spectroscopy. *Biochimica Et Biophysica Acta-General Subjects.* **1724,** 262-269.

18. Stuart, B. (2000) Infrared spectroscopy. *Kirk-Othmer Encyclopedia of Chemical Technology.* 1-18.

19. Nakazawa, I. and Iwaizumi, M. (1989) A role of the cancer cell membrane fluidity in the cancer metastases: an ESR study. *Tohoku J. Exp. Med.* **157,** 193-198.

20. Sade, A., Tuncay, S., Cimen, I., Severcan, F. and Banerjee, S. (2012) Celecoxib reduces fluidity and decreases metastatic potential of colon cancer cell lines irrespective of COX-2 expression. *Biosci. Rep.* **32,** 35-44.

21. Pevsner, A. and Diem, M. (2001) Infrared spectroscopic studies of major cellular components. Part I: the effect of hydration on the spectra of proteins. *Appl. Spectrosc.* **55,** 788-793.

22. YANG, D., CASTRO, D.J., EL-SAYED, I.H., EL-SAYED, M.A., SAXTON, R.E. and ZHANG, N.Y. (1995) A Fourier-transform infrared spectroscopic comparison of cultured human fibroblast and fibrosarcoma cells: a new method for detection of malignancies. *J. Clin. Laser Med. Surg.* **13,** 55-59.

23. Eckel, R., Huo, H., Guan, H., Hu, X., Che, X. and Huang, W. (2001) Characteristic infrared spectroscopic patterns in the protein bands of human breast cancer tissue. *Vibrational Spectroscopy.* **27,** 165-173.

24. Wald, N. and Goormaghtigh, E. (2015) Infrared imaging of primary melanomas reveals hints of regional and distant metastases. *Analyst.* **140,** 2144-2155.

25. Brannon, A.R., Vakiani, E., Sylvester, B.E., Scott, S.N., McDermott, G., Shah, R.H., Kania, K., Viale, A., Oschwald, D.M. and Vacic, V. (2014) Comparative sequencing analysis reveals high genomic concordance between matched primary and metastatic colorectal cancer lesions. *Genome Biol.* **15,** 454.

26. Turajlic, S., Furney, S.J., Lambros, M.B., Mitsopoulos, C., Kozarewa, I., Geyer, F.C., Mackay, A., Hakas, J., Zvelebil, M., Lord, C.J., Ashworth, A., Thomas, M., Stamp, G., Larkin, J., Reis-Filho, J.S. and Marais, R. (2012) Whole genome sequencing of matched primary and metastatic acral melanomas. *Genome Res.* **22,** 196-207.

27. Hyo-eun, C.B., Ruddy, D.A., Radhakrishna, V.K., Caushi, J.X., Zhao, R., Hims, M.M., Singh, A.P., Kao, I., Rakiec, D. and Shaw, P. (2015) Studying clonal dynamics in response to cancer therapy using high-complexity barcoding. *Nat. Med.* **21,** 440.

28. Jamal-Hanjani, M., Quezada, S.A., Larkin, J. and Swanton, C. (2015) Translational implications of tumor heterogeneity. *Clin. Cancer Res.* **21,** 1258-1266.

29. Somasundaram, R., Villanueva, J. and Herlyn, M. (2012) Intratumoral heterogeneity as a therapy resistance mechanism: role of melanoma subpopulations. In: *Advances in pharmacology,* Anonymous Elsevier. pp 335-359.

30. Fattore, L., Ruggiero, C.F., Liguoro, D., Mancini, R. and Ciliberto, G. (2019) Single cell analysis to dissect molecular heterogeneity and disease evolution in metastatic melanoma. *Cell death & disease.* **10,** 1-12.